An easy way to controllably synthesize one-dimensional SmB_6 topological insulator nanostructures and exploration of their field emission applications*

Xun Yang(杨汛), Hai-Bo Gan(甘海波), Yan Tian(田颜), Ning-Sheng Xu(许宁生), Shao-Zhi Deng(邓少芝), Jun Chen(陈军), Huanjun Chen(陈焕君), Shi-Dong Liang(梁世东), and Fei Liu(刘飞)†

State Key Laboratory of Optoelectronic Materials and Technologies, Guangdong Province Key Laboratory of Display Material and Technology, School of Electronics and Information Technology, Sun Yat-sen University, Guangzhou 510275, *China*

(Received 7 August 2017; revised manuscript received 16 August 2017; published online 30 September 2017)

A convenient fabrication technique for samarium hexaboride (SmB_6) nanostructures (nanowires and nanopencils) is developed, combining magnetron-sputtering and chemical vapor deposition. Both nanostructures are proven to be single crystals with cubic structure, and they both grow along the [001] direction. Formation of both nanostructures is attributed to the vapor-liquid-solid (VLS) mechanism, and the content of boron vapor is proposed to be the reason for their different morphologies at various evaporation distances. Field emission (FE) measurements show that the maximum current density of both the as-grown nanowires and nanopencils can be several hundred $\mu A/cm^2$, and their FN plots deviate only slightly from a straight line. Moreover, we prefer the generalized Schottky–Nordheim (SN) model to comprehend the difference in FE properties between the nanowires and nanopencils. The results reveal that the nonlinearity of FN plots is attributable to the effect of image potential on the FE process, which is almost independent of the morphology of the nanostructures. All the research results suggest that the SmB_6 nanostructures would have a more promising future in the FE area if their surface oxide layer was eliminated in advance.

Keywords: one-dimensional SmB_6 nanostructures, chemical vapor deposition (CVD), field emission (FE), image potential

PACS: 81.07.–b, 81.15.Gh, 79.70.+q, 73.20.–r **DOI:** 10.1088/1674-1056/26/11/118103

1. Introduction

In recent years, nanostructures[1–8] are intensively investigated because they exhibit more fascinating properties than their bulk counterparts. Among them, SmB_6 nanostructures have attracted considerable attention because they are typical Kondo topological insulators,[9–11] which are predicted to have abundant surface electronic states. But due to the anisotropy and high stability of SmB_6, synthesis methods for one-dimensional SmB_6 nanostructures are rather few. To our knowledge, either poisonous BCl_3 gas[12] or inflammable $B_{10}H_{14}$ gas[13] is usually chosen as the boron source for recently reported synthesis of SmB_6 nanowires, which inevitably implies harsh growth conditions. So it is a great challenge for researchers to find a moderate way to controllably prepare high-quality single-crystalline SmB_6 nanostructures. In addition, SmB_6 nanostructures may have potential applications in field emission (FE) areas because they not only have superb surface electron states but also have low electrical resistivity (2.07×10^{-4} Ω·cm), low work function (4.4 eV), high melting point (2580 °C), and high thermal conductivity (13.8 $W\cdot m^{-1}\cdot K^{-1}$).[14–17] Although some effort has been devoted to investigating their FE behaviors, the nature of their emission mechanism has not been thoroughly understood, which inhibits rapid progress in their FE applications.

In this paper, we report developing a convenient CVD method to fabricate single-crystalline SmB_6 nanostructures (nanowires and nanopencils) under control. Moreover, the FE properties of the SmB_6 nanowire and nanopencil films are compared in order to comprehend their intrinsic emission mechanisms. Finally, the generalized Schottky–Nordheim (SN) model is utilized to explain their different emission behaviors.

2. Experiment

The synthesis of SmB_6 nanostructures was conducted in a horizontal tube-furnace by a simple low-pressure CVD method, as described in our previous publications.[2,18,19] Mixed B and B_2O_3 powders were used as boron sources, both of which are nontoxic and environment-friendly. They were loaded into a vessel and placed in the central region of the furnace. Sm (200 nm) and Ni (10 nm) films were respectively deposited onto the surface of Si substrate by magnetron sputtering, serving as the Sm material and catalyst of the nanostructure growth. The deposition parameters of these films are

*Project supported by the National Key Basic Research Program of China (Grant No. 2013CB933601), National Project for the Development of Key Scientific Apparatus of China (Grant No. 2013YQ12034506), the Fundamental Research Funds for the Central Universities of China, the Science and Technology Department of Guangdong Province, China, the Education Department of Guangdong Province, China, and the Natural Science Foundation of Guangdong Province, China (Grant No. 2016A030313313).

†Corresponding author. E-mail: liufei@mail.sysu.edu.cn

© 2017 Chinese Physical Society and IOP Publishing Ltd

summarized in Table 1. The synthesis procedures of the SmB_6 nanostructures can be depicted as follows. First, the furnace was rapidly heated to 700 °C and kept there for an hour in the mixed gas of Ar (285 sccm) and H_2 (200 sccm). Secondly, when the temperature reached 1100 °C, the growth of the SmB_6 nanostructures was initiated. In this stage, the flow rate of H_2 was reduced to 30 sccm and the chamber pressure was kept at about 0.3–0.5 kPa. The whole reaction lasted about 2–4 hours. Finally, a dark film was found on the surface of the Si substrate after the furnace was cooled down to room temperature under the protection of Ar gas.

X-ray diffractometry (Rigaku, D-MAX 2200 VPC) and Raman spectroscopy (Renishaw, Invia Reflex) were used to ascertain the chemical compositions of the products. The morphology and crystalline structure of the samples were respectively characterized by scanning electron microscope (SEM, Zeiss, SUPER-55) and transmission electron microscope (TEM, FEI, Titan 3 G260-300). And the FE measurements of the SmB_6 nanostructure films were performed in our own custom built FE analysis and measurement system.

Table 1. Deposition parameters for the Sm and Ni thin films.

Film	Gas flow rate/sccm	Power/W	Time/min.	Base pressure/Pa	Thickness/nm
Sm	Ar (100)	90	4.85	6×10^{-4}	200
Ni	Ar (100)	200	4.8	6×10^{-4}	10

3. Results and discussion

By adjusting the evaporation distance between the boron sources and the substrate, aligned SmB_6 nanowires and nanopencils have been successfully fabricated on the Si substrate, respectively. SEM images of the SmB_6 nanostructures are shown in Fig. 1. Typical side- and top-view images of SmB_6 nanowires are presented in Figs. 1(a) and 1(b), in which one can see that the nanowires have an average length of 5 μm, and their mean diameter is about 175 nm. Moreover, the nanowires have a uniform diameter from the top to the base, as seen in Fig. 1(b). Figures 1(c) and 1(d) are SEM images of the SmB_6 nanopencils. The mean length of the nanopencils is about 2 μm. The diameter of the nanopencils tapers gradually from 190 nm to 65 nm along the growth direction. Because their shape resembles a pencil, they are called nanopencils. To further compare these nanostructures, other morphology parameters are summarized in Table 2. From Fig. 1, the SmB_6 nanostructures with identical morphology (nanowires or nanopencils) are seen to be distributed uniformly all over the substrate, which suggests that our synthesis method has nice controllability for the formation of SmB_6 nanostructures. Moreover, the surface of the nanostructures is very smooth and the catalyst particles are found on their tips for both the SmB_6 nanowires and nanopencils. Table 2 shows that the mean length (5 μm) of the nanowires is obviously larger than that (2 μm) of the nanopencils, which may result from the boron vapor pressure at different evaporation distances.

Table 2. Morphology parameters of the SmB_6 nanowires and nanopencils.

Morphology	Mean diameter/nm	Mean length/μm	Growth density/cm^{-2}	Evaporation distance/cm	Aspect ratio
SmB_6 nanowires	175	5	4×10^7	3	28.6
SmB_6 nanopencils	65 (top) 190 (end)	2	1×10^8	7.5	30.8

Considering that the Ni catalysts are used in the growth process of both the SmB_6 nanowires and nanopencils, we prefer to use the vapor-liquid-solid (VLS) mechanism[20] to explain the effect of the evaporation distance on the formation of different nanostructures. The possible explanations can be depicted as follows. First, the 10 nm continuous Ni film will turn into discrete catalyst nanoparticles after an hour's pretreatment at 700 °C. Meanwhile, some Sm atoms from the Sm film will gradually dissolve into the catalysts to form the Sm/Ni alloy nanoparticles due to their solid-state interdiffusion. Secondly, when the temperature is raised to 1000 °C, B_2O_2 vapor[2,21] is generated by the reaction of B and B_2O_3 powders, which will be transferred to the substrate region under the function of carrier gas. Third, the B_2O_2 vapor reacts with the Sm/Ni alloy droplets and produces the SmB_6 phase with the help of the Ni catalysts. Subsequently, when the solubility of the SmB_6 phase in the alloy droplets arrives at oversaturation with the proceeding of the reaction, the SmB_6 solids will precipitate from the alloy droplets and form on the surface of the Si substrate, acting as the nuclei of the growth of the nanostructures. Finally, with the continuous precipitation of SmB_6 from the alloy droplets, the SmB_6 solid gradually forms one-dimensional nanostructures along the energy-favorable direction. Based on our analysis, two main factors must be responsible for the formation of the SmB_6 nanopencils and nanowires. One is the growth temperature, because the temperature of the substrate with a 7.5 cm evaporation distance is 80 °C lower than that of the substrate with a 2.5 cm evapora-

tion distance. As is known to us all, the lattice face vertical to the growth axis usually possesses the highest growth rate when the growth temperature is lower than a critical temperature because they have the highest surface energy. Under this circumstance, the diameter of the nanostructures decreases from the bottom to the top and the nanopencils are produced, which results from the rapid growth of the preferred face. But when the growth temperature is higher than some critical temperature, the growth speed of every lattice face tends to be equal for nanostructures, which leads to the formation of the nanowires with uniform diameter along their length. The other is the vapor pressure of the B_2O_2 because the evaporation distance between the source materials and the substrate is different for the formation of nanowires (3 cm) versus nanopencils (7.5 cm). With lengthening the diffusing distance of the B_2O_2, the vapor pressure will accordingly decrease. So this factor will also affect the formation of the SmB_6 nanostructures. Moreover, our mechanism is also consistent with the growth mechanism of the LaB_6 nanoobelisks[22] and ZnO nanotips.[23] So it is reasonable that the discrepancy of boron vapors at varied evaporation distances should be the intrinsic factor for the formation of different morphology of SmB_6 nanostructures. The thickness of the Ni film can also affect the formation of the nanostructures. In our experiments, the thickness of the Ni film is adopted to vary from 8 nm to 15 nm. If the thickness of the Ni film is lower than 8 nm, only the SmB_6 nanoparticles can be found on the substrate instead of the nanowires or nanopencils. But when the thickness of the catalysts is higher than 15 nm, the growth density of the nanostructures decreases. Therefore, the most suitable thickness of the Ni film is between 8 nm and 15 nm. The detailed mechanism is still under research.

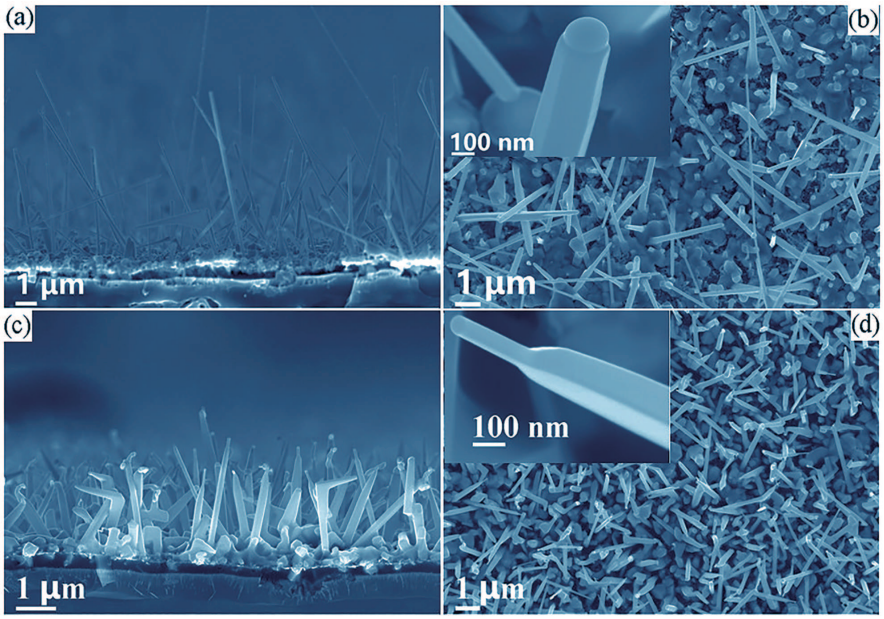


Fig. 1. (a), (b) Side- and top-view SEM images of the SmB_6 nanowires. (c), (d) Typical morphology images of the SmB_6 nanopencils. The insets are high-magnification cross-sectional images.

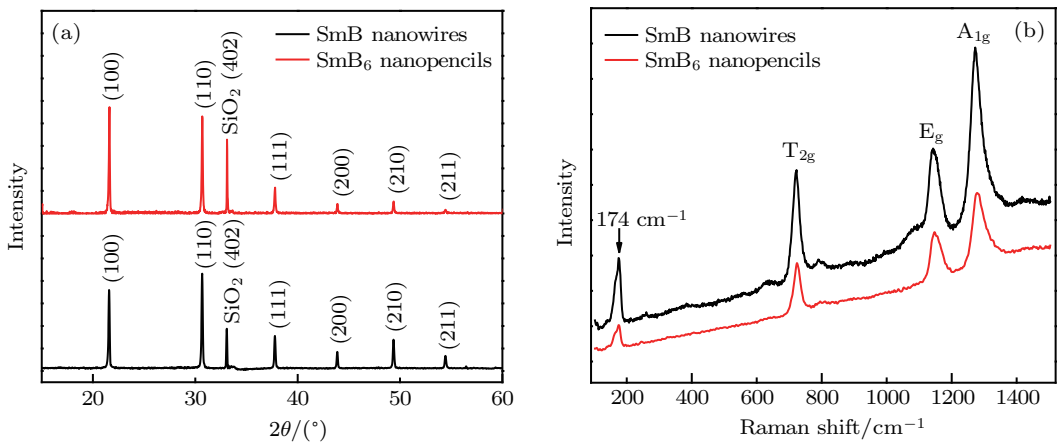


Fig. 2. (color online) (a) Typical XRD patterns and (b) Raman spectra of the SmB_6 nanowires and nanopencils.

In order to confirm the chemical compositions of the as-prepared nanostructures, x-ray diffraction (XRD) and Raman spectroscopy were subsequently performed on the samples. It is found in Fig. 2(a) that nearly all of the diffraction peaks agree well to those of the SmB_6 phase according to the standard JCPDS Card No. 24-1120, except the [402] peak of SiO_2 resulting from the native oxidation layer of the silicon substrate. Figure 2(b) gives the Raman spectra of these two samples. There are four characteristic peaks in the spectra of the nanowires or nanopencils, which are 174 cm^{-1}, 721 cm^{-1}, 1142 cm^{-1}, and 1272 cm^{-1}. The peak at 174 cm^{-1} may originate from the vibration of the Sm ions in the cage formed by the B_6 molecule,[4,24] and the peak at 721 cm^{-1} belongs to T_{2g} vibrational mode.[25,26] The peaks at 1142 cm^{-1} and 1272 cm^{-1} are attributed to the E_g and A_{1g} modes,[25,26] respectively. Combining the XRD with the Raman results, both the nanowires and nanopencils can be indexed as pure SmB_6 crystals.

TEM images of the SmB_6 nanowires and nanopencils are given in Fig. 3 to further ascertain their crystallinity and growth direction. It is clear in Figs. 3(a) and 3(d) that the diameter is nearly unvaried along the growth direction for the nanowires, whereas the diameter decreases from the end to the top for the nanopencils, which conforms to the SEM results (Fig. 1). The inset gives the corresponding EDX mapping spectra, which reveal that the Sm and B elements are distributed uniformly along the growth direction for both nanostructures. Figures 3(b) and 3(e) respectively give typical SAED patterns of the nanowire and nanopencil, in which one can see that their diffraction spots are very sharp and clear. Moreover, the high-resolution TEM images of the nanowire and nanopencil are provided in Figs. 3(c) and 3(f). It is found that the lattice distance between adjacent growth planes is about 0.41 nm for both nanostructures, which is in good agreement with the interplanar spacing of cubic SmB_6 crystals along the [001] orientation. Note that a very thin amorphous shell exists on the surface of the nanostructures, whose thickness is usually less than 1 nm. Based on the TEM, SAED, and EDX mapping spectra, it can be concluded that the as-grown nanowires and nanopencils are both cubic SmB_6 single crystals with a growth direction of [001].

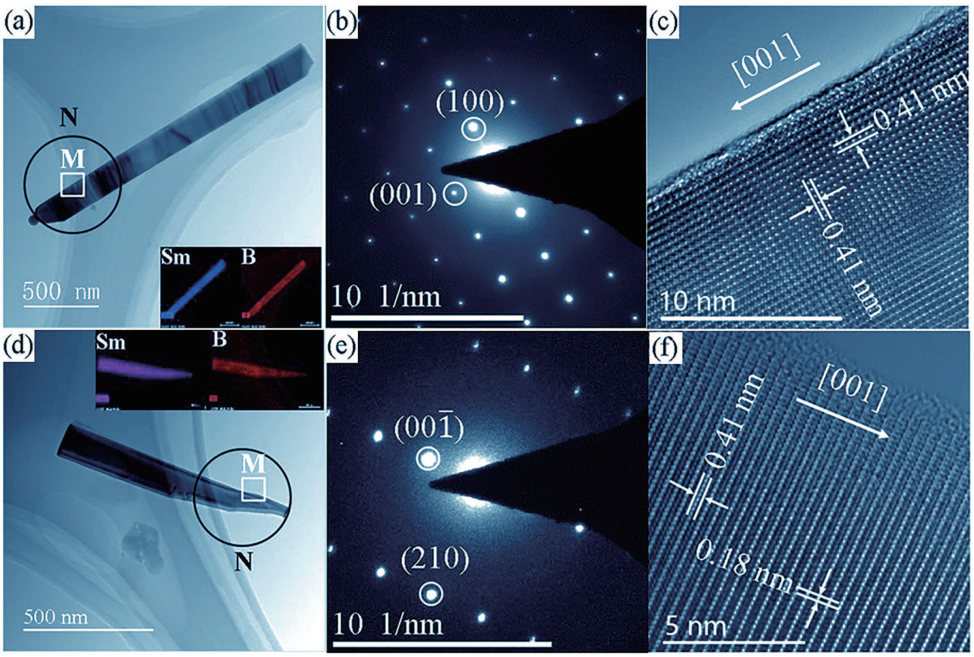


Fig. 3. (color online) (a)–(c) TEM images and SAED pattern of an SmB_6 nanowire. The Sm and B elemental maps are shown in the inset. (d)–(f) TEM and EDX mapping analysis of the SmB_6 nanopencil.

Field emission measurements of the SmB_6 nanostructure film were carried out in our FE analysis and measurement system custom built in-house, in which ITO glass served as the anode. The areas of the nanowire and nanopencil films were respectively 0.49 cm^2 and 0.20 cm^2, and the distance between cathode and anode was kept at about 280 μm throughout the measurements. The chamber pressure was about 3.5×10^{-5} Pa and the transparent anode method was used to research on the samples. The field current density (J) versus electric field (E) curves and Fowler–Nordheim (FN) plots of the nanowires and nanopencils are shown in Figs. 4(a) and 4(b), respectively. One can see in Fig. 4(a) that the SmB_6 nanowires have a lower turn-on field of 6.5 V/μm (at 10 μA/cm^2) compared with that of the nanopencils (6.9 V/μm), and their maximum emission current density can reach several hundred μA/cm^2. The inset gives the corresponding field emission images, in which one can find that the emission uniformity of the nanowires is better than that of the nanopencils. As seen in Table 1, the growth

density and the aspect ratio of the nanowires and nanopencils are very close, which cannot be used to elucidate their different emission behaviors. Our experiments find that the nanopencils usually burn up during high-current treatments. Because the sharp tips of the nanopencils have much higher resistance than other regions, the heat production at high-resistance region is so huge that these tips are first to burn out at large emission currents, which lowers the number of emission sites. So it is comprehensible that the SmB_6 nanowires display better emission performance than the nanopencils.

In addition, it is seen in Fig. 4(b) that the FN plots of both SmB_6 nanostructures exhibit a little nonlinear characteristic, which suggests that the FE mechanism of the SmB_6 nanostructures may deviate from the traditional FN theory. Here, the generalized SN model[27] is utilized to explain the nonlinear behaviors of the FN plots for the SmB_6 nanostructures. Figure 5(a) gives the curves of emission current density of the SmB_6 nanostructures versus the applied field, in which the matching degree of the experimental curves to the fitting curves is over 0.99. Table 3 lists the curve-fitting parameters in order to compare their field emission behaviors further. It is obvious that the two nanostructures' fitting parameter a_{FN} differs, which is far lower than the constant (1.54 $\mu A{\cdot}eV{\cdot}V^{-2}$) in the classical FN equation. We prefer the following illustrations to comprehend the change of parameter a_{FN}. In the calculation, FE current density J can be deduced by the expression $J = I/S$, where S is the total area of the SmB_6 nanostructure film on the substrate. Because more or less uniformity must exist in the distribution and the field screening effect of the SmB_6 nanostructures on substrate, only a very small number of SmB_6 nanostructures on the substrate contribute to FE current in measurements. As a result, it is reasonable that parameter a_{FN} is significantly smaller than the constant parameter and varies with the actual emission area of SmB_6 nanostructures because it truly reflects the difference between the actual area of nanostructures involved in emission and the total film area. Moreover, it is obvious that the parameter a_{FN} of the nanowires is greater than that of the nanopencils in our calculations, which agrees to the measurement results of field emission images (Fig. 4(a)). One can also see that the field enhancement factor (β) is similar for SmB_6 nanowires ($\beta = 996$) and nanopencils ($\beta = 1150$), which suggests that β should have little effect on the difference of their FE properties.

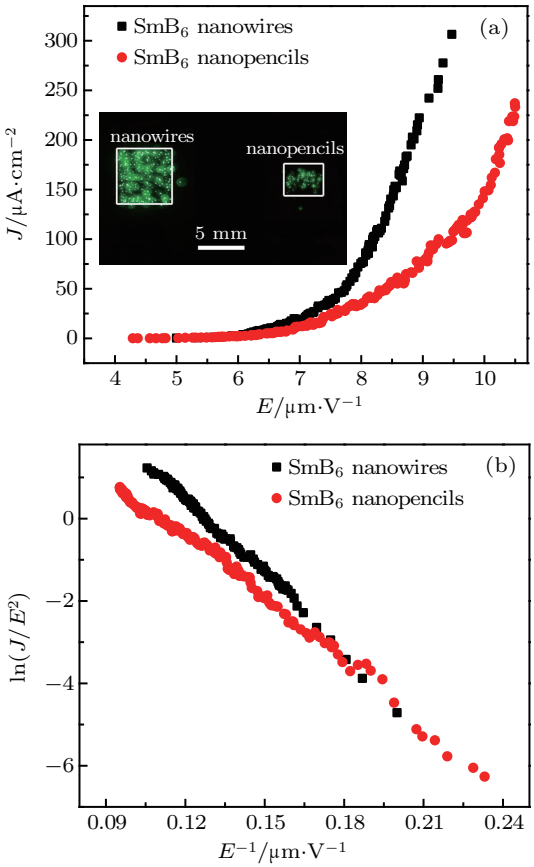


Fig. 4. (color online) (a) FE current density-electric field (J–E) curves of the SmB_6 nanowires and nanopencils. The inset shows emission images of the nanostructures. (b) The corresponding FN plots.

Table 3. Nonlinear fitting parameters of the experimental J–E curves for SmB_6 nanostructures.

Nanomaterials	Nonlinear fitting parameters				
	$a_{FN}/\mu A{\cdot}eV{\cdot}V^{-2}$	Φ/eV	β	λ	Conduction-type
SmB_6 nanowires	8.1×10^{-13}	4.4	996	1	metallic
SmB_6 nanopencils	9.2×10^{-14}	4.4	1150	1	metallic

Figures 5(b) and 5(c) respectively give their corresponding FN plots and partial derivative curves. One can see in Fig. 5(b) that the FN plots of both SmB_6 nanowires and nanopencils exhibit a slight deviation from linearity, which implies that the existence of the image potential may affect their FE process. Further, it can be found in Fig. 5(c) that the first derivative curves of SmB_6 nanostructures show a decreasing tendency with the increase of $1/F$, which proves the existence of the nonlinearity of the FN plots in Fig. 5(b). From Fig. 5(d), the slope S_{GSN} of the FN plots is found to increase linearly with the effective electric field F for both the SmB_6 nanowires and nanopencils. This result agrees with the ideal SN model, in which the surface charges at the interface should be equal to the mirror charges at the vacuum side for metals. Given that, the image potential parameter λ is set to 1, which reflects that ideal image potential exists in the field emission process for both the SmB_6 nanowires and nanopencils. Based on the generalized SN model, both the SmB_6 nanowires and nanopen-

cils can be determined to be metals, like their bulk counterparts. Because the SmB_6 nanostructures are determined to have metallic properties, the image potential must be mainly responsible for the nonlinearity of the FN plots of both nanostructures. As intrinsic Kondo topological insulators, the SmB_6 nanostructures should exhibit more excellent FE performance than observed in our experiments because they are predicted to have abundant surface states and ultra-high surface electron mobility. We speculate that the existence of the amorphous oxide layer keeps the electrons from rapid transporting along the surface of the nanowires or nanopencils and dominates the FE process instead of the superb surface states, which leads to the worse than expected emission performance. In future work, we will endeavor to get rid of the surface oxide layer of the SmB_6 nanostructures, allowing them to exhibit their intrinsic excellent emission properties.

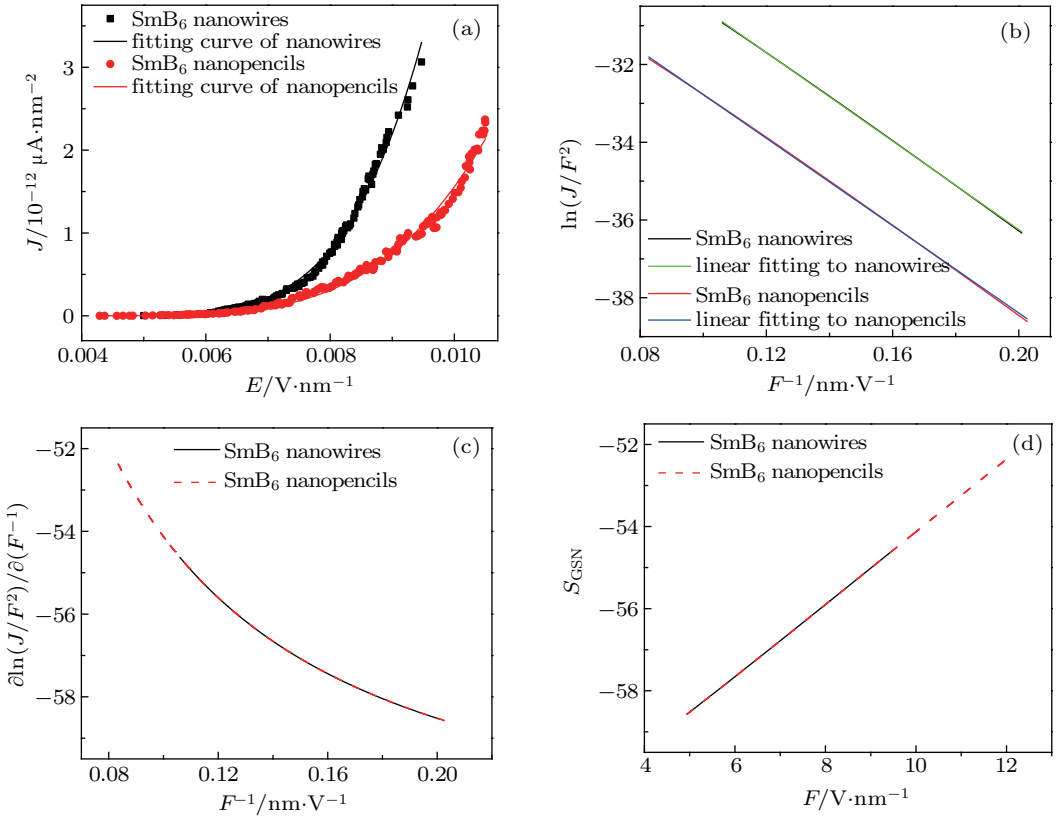


Fig. 5. (color online) (a) Fitting J–E curves of the SmB_6 nanostructures, (b) corresponding FN plots, (c) curves of the partial derivative of the FN plots to $1/F$, (d) curves of the FN plots' slope versus the effective electric field.

4. Conclusion

In summary, SmB_6 nanostructures (nanowires and nanopencils) have been successfully fabricated on Si substrate via a convenient CVD method. Both the as-prepared SmB_6 nanowires and nanopencils are indexed as single crystals with cubic structure, which grow along the [001] direction. FE measurements show that the field emission behaviors of SmB_6 nanowires are better than those of SmB_6 nanopencils, which may result from higher endurance under large current for the nanowires. Moreover, the generalized SN model is used to explain the nonlinear behaviors of the FN plots of the SmB_6 nanowires and nanopencils, in which the effect of image potential on FE process is carefully discussed. To better exhibit the excellent emission properties of SmB_6 as an ideal Kondo topological insulator, the surface oxide shell of the nanostructures must be eliminated in advance.

References

[1] Liu F, Su Z, Mo F, Li L, Chen Z, Liu Q, Chen J, Deng S and Xu N 2011 *Nanoscale* **3** 610
[2] Liu F, Tian J, Bao L, Yang T, Shen C, Lai X, Xiao Z, Xie W, Deng S and Chen J 2008 *Adv. Mater.* **20** 2609
[3] Shen Y, Xu N, Deng S, Zhang Y, Liu F and Chen J 2014 *Nanoscale* **6** 4659
[4] Xu J, Hou G, Li H, Zhai T, Dong B, Yan H, Wang Y, Yu B, Bando Y and Golberg D 2013 *NPG Asia Mater.* **5** e53
[5] Zhang Z, Song X, Chen Y, She J, Deng S, Xu N and Chen J 2017 *J. Alloys Compd.* **690** 304
[6] Wu D, Cheng H, Zheng X, Wang X, Wang D and Li J 2015 *Chin. Phys. Lett.* **32** 108102
[7] Li J, Gao Z, Xue X, Li H, Deng J, Cui B and Zou D 2016 *Acta Phys. Sin.* **65** 118104 (in Chinese)
[8] Shen Z, Chen C, Wang R, Wang B and Yan H 2016 *Acta Phys. Sin.* **65** 236803 (in Chinese)
[9] Hatnean M C, Lees M R, Paul D M and Balakrishnan G 2013 *Sci. Rep.* **3** 3071
[10] Kim D J, Xia J and Fisk Z 2014 *Nat. Mater.* **13** 466
[11] Lu F, Zhao J, Weng H, Fang Z and Dai X 2013 *Phys. Rev. Lett.* **110** 096401
[12] Xu J, Zhao Y, Shi Z, Zou C and Ding Q 2008 *J. Cryst. Growth.* **310** 3443

[13] Brewer J R, Jacobberger R M, Diercks D R and Cheung C L 2011 *Chem. Mater.* **23** 2606
[14] Berchmans L J, Visuvasam A, Angappan S, Subramanian C and Suri A 2010 *Ionics* **16** 833
[15] Ji X, Zhang Q, Xu J and Zhao Y 2011 *Prog. Solid State Chem.* **39** 51
[16] Nickerson J, White R, Lee K, Bachmann R, Geballe T and Hull Jr G 1971 *Phys. Rev. B* **3** 2030
[17] Xu J, Zhao Y, Ji X, Zhang Q and Lau S 2009 *J. Phys. D: Appl. Phys.* **42** 135403
[18] Liu F, Gan H, Tang DM, Cao Y, Mo X, Chen J, Deng S, Xu N, Golberg D and Bando Y 2014 *Small* **10** 685
[19] Liu F, Tang D M, Gan H, Mo X, Chen J, Deng S, Xu N, Bando Y and Golberg D 2013 *ACS Nano* **7** 10112
[20] Wagner R and Ellis W 1964 *Appl. Phys. Lett.* **4** 89
[21] Gan H, Peng L, Yang X, Tian Y, Xu N, Chen J, Liu F and Deng S 2017 *RSC Adv.* **7** 24848
[22] Brewer J R, Deo N, Morris W Y and Cheung C L 2007 *Chem. Mater.* **19** 6379
[23] Ye Z, Huang J, Xu W, Zhou J and Wang Z 2007 *Solid State Commun.* **141** 464
[24] Ogita N, Nagai S, Udagawa M, Iga F, Sera M, Oguchi T, Akimitsu J and Kunii S 2005 *Phys. B* **359** 941
[25] Mörke I, Dvorak V and Wachter P 1981 *Solid State Commun.* **40** 331
[26] Ogita N, Nagai S, Okamoto N, Udagawa M, Iga F, Sera M, Akimitsu J and Kunii S 2003 *Phys. Rev. B* **68** 224305
[27] Yang X, Gan H B, Tian Y, Peng L X, Xu N S, Chen H J, Chen J, Deng S Z, Liang S D and Liu F 2017 unpublished